Dialogue Social Science Review (DSSR)
www.thedssr.com

ISSN Online: 3007-3154
ISSN Print: 3007-3146

DIALOGUE SOCIAL SCIENCE REVIEW

Vol. 3 No. 2 (February) (2025)

A Variational based Model for Edge Detection Using Local Meshless Method

Muhammad Atif
Department of natural science and humanities, university on engineering Mardan KP, Pakistan

Mushtaq Ahmad Khan (Corresponding Author)
Department of natural science and humanities, university on engineering Mardan KP, Pakistan. Email: mushtaq@uetmardan.edu.pk

Abdul Kabir
Department of natural science and humanities, university on engineering Mardan KP, Pakistan

Fazal Amin
Department of natural science and humanities, university on engineering Mardan KP, Pakistan

Abstract
This article presents the Local Meshless Method (LMM) for numerically solving Partial Differential Equations (PDEs) conncected with a Total Variation (TV) regularization-based edge detection model. The suggested meshless method not only restores images but also effectively preserves edges. This advantage arises from its independence from mesh generation, allowing it to handle complex geometries, significant irregularities, and discontinuities. Experimental results show that the proposed meshless method achieves excellent results in terms of image denoising, specifically measured by Signal to Noise Ratio (SNR), and edge detection, evaluated using the Edge Preservation Index (EPI), when compared to traditional mesh-based methods.

Key words: Edge detection, TV- Regularization, Euler-Lagrange PDE (EL-PDE), Radial Basis Function (RBF) Interpolation, SNR, EPI, Filters, Multiquadric Basis Function

Introduction

Edge detection is a necessary task in Computer vision and image processing. It is an important component used to identify the boundaries within images. Edge detection is a challenging task when additive noise is concerned and when several edges bisect and are close together. The additive noise removal model is given below.

$$H_\jmath = F + \mathfrak{A}\,, \tag{1}$$

where $H_\jmath: \Omega \subset R \to R^2$ is given the noisy image having additive noise $\mathfrak{A}$ and E is the true image. Edge detection is important because it simplifies image data, reducing the volume of information that needs to be processed while retaining the essential structural

Dialogue Social Science Review (DSSR)
www.thedssr.com

ISSN Online: 3007-3154
ISSN Print: 3007-3146

DIALOGUE SOCIAL SCIENCE REVIEW

Vol. 3 No. 2 (February) (2025)
features of objects within the image. Edges provide crucial information for various subsequent visual tasks, including image recognition [1,2,3,4], image segmentation [5,6,7], image retrieval [9,10], face recognition [11,12,13], corner detection [14,15], road detection [16], and target tracking [17]. In the field of medical imaging, significant features are extracted from the retina of the human eye, including the length, breadth, and angle of blood vessels, using edge detection [18]. In the literature, edge detection is considered to carry the most important information in an image. Many strategies have been employed by researchers for image edge detection, resulting in effective image restoration and edge preservation. However, these techniques have limitations concerning edge detection and edge preservation. For further details, see [19,20,21]. Recent advancements in TV-regularization-based PDE models for edge detection have demonstrated effective outcomes in image denoising and edge detection. The first model for edge detection based on TV regularization and connected PDE is introduced and explained in reference [22]. Recently, various mesh-based techniques have been employed to address challenges in image edge detection, leading to some promising results. For detailed information, refer to sources [26, 27, 28, 29, 30, 31, 32]. However, image edge detection still encounters difficulties due to the associated EL-PDE, which is nonlinear and non-differentiable. Therefore, in this article, we utilize the Local Meshless Method (LMM) to mitigate these challenges and achieve a smoother solution. For more information, refer to sources [22, 23, 24] regarding models based on TV regularization. Peter et al. [25] introduced the first model for edge detection in images with additive noise using TV-based regularization. This model generates a PDE that is always nonlinear and non-differentiable. The results obtained using traditional schemes related to the TV-based edge detection model yield very satisfactory outcomes for image restoration while preserving edges. However, it also has some adverse properties, such as loss of image contrast in restoration, which leads to poor edge detection and increased computation time due to its nonlinearity and non-differentiability. For more details, readers are referred to [25]. Recently, various mesh-based schemes have been employed to address these challenges, resulting in improved outcomes for image edge detection. For further detail, see [26, 27, 28,29, 30 31, 32]. But still, image edge detection faces difficulties due to the associated EL-PDE, which is nonlinear and non-differentiable. In this article, we utilize the Local Meshless Method (LMM) to overcome the aforementioned challenges and achieve a smooth solution.

Researchers have recently demonstrated that RBF interpolation methods are effective mesh-free techniques in both approximation theory and the numerical solutions of PDEs. The use of RBFs for interpolation has the advantage of being applicable to multidimensional scattered data [33, 34]. Meshless methods based on Radial Basis Function (RBF) interpolation have consistently shown superior results across various challenges, yielding smooth outcomes in both scientific and engineering applications [35, 36, 37]. The choice of the shape parameter often influences the results, with several basis functions commonly employed in RBF interpolation, including Multiquadric (MQ), Gaussian (GA), Inverse Multiquadric (IMQ), and Polyharmonic spline. For additional information, refer to [38, 39]. The appeal of RBF techniques stems from its meshless applications, which discretize continuous problems using just a collection of points. Adding this feature to the RBF technique is simple, particularly for problems

Dialogue Social Science Review (DSSR)
www.thedssr.com

ISSN Online: 3007-3154
ISSN Print: 3007-3146

DIALOGUE SOCIAL SCIENCE REVIEW

Vol. 3 No. 2 (February) (2025)

with complex shapes and multiple dimensions. The RBF methods are free of meshes and highly precise, making them effective for producing smooth solutions in complex geometries. The main advantage of numerical methods commented with RBFs over traditional approaches is the absence of a mesh, resulting in higher performance than Finite Difference Scheme (FDM) [42,43], the Finite Element Method (FEM) [42], the Finite Volume Method (FVM) [41,44,45)], and the Pseudo-Spectral Method [46] in terms of spectral accuracy [47] and exponential convergence [48]. Hence the meshless approaches are superior to conventional methods regarding the smooth solution. For further information on RBF collocation techniques, see [49, 50, 51,52,53,54,55].

Hardy et al. proposed the Local Meshless Method (LMM) for the numerical solution of partial differential equations (PDEs) [56]. Later, he demonstrated through various numerical solutions of partial differential equations (PDEs) that the multi-quadratic radial basis function (MQ-RBF) is the most effective basis function for numerically solving different types of PDEs compared to other basis functions. The Local Meshless Method (LMM) is user-friendly, offers a high level of accuracy, and exhibits exponential convergence when solving partial differential equations (PDEs). Due to its adaptive characteristics, effective computational approach, and straightforward mathematical implementation, the LMM can solve PDEs more quickly and efficiently than conventional mesh-based methods. This proposed meshless technique is especially advantageous for obtaining smooth solutions to both linear and non-linear PDEs.

Inspired by the application of LMM, we will utilize it on the time-dependent EL-PDE associated with TV-based model for image edge detection. This approach aims to achieve a smooth solution for both image edge detection and image denoising. The use of LMM will enhance not only the effectiveness of image edge detection but also improve image denoising due to its various applications.

The rest of the article is organized as follows. Section 2 presents related work. The first subsection includes a brief mathematical discussion of the TV-based edge detection model, while the second subsection discusses BRF interpolation. Section 3 focuses on the mesh-based gradient descent numerical scheme for solving the EL-PDE in connection with the TV-based edge detection model. This section also introduces the proposed LMM scheme for achieving a smooth numerical solution of the EL-PDE associated with the edge detection model. Section 4 describes the experimental results and discussions of the proposed LMM in comparison with traditional edge detection methods. Finally, the conclusion is presented in Section 5.

Background Knowledge

Total Variation-Based Edge Detection Model

Peter et al. [25] introduced the first model for image edge detection in the presence of additive noise by utilizing TV regularization. This model has shown promising results in both image edge detection and denoising, thanks to the inherent edge-detecting capabilities of TV regularization. The mathematical framework for edge detection and image restoration provided by Peter et al. [25] is presented in equation (1) below.

$$\hat{F} = argmin_E X(F) = TV(F) = \int_\Omega |\nabla F| \, dxdy \, , where \, |\nabla F| = \sqrt{F_x^2 + F_y^2} \, , \qquad (2)$$

Dialogue Social Science Review (DSSR)
www.thedssr.com

ISSN Online: 3007-3154
ISSN Print: 3007-3146

DIALOGUE SOCIAL SCIENCE REVIEW

Vol. 3 No. 2 (February) (2025)

where F represent restored image have additive noise (salt and paper noise) 𝔄 from given noisy image Ⱨ as mentioned in equation (1). The associated PDE of equation (2) is given follow.

$$-\nabla\left(\frac{\nabla F}{|\nabla F|+\varepsilon}\right)=0 \text{ in } \Omega \text{ for } \epsilon>0,(x,y)\in R^2. \quad (3)$$

Equation (3) can be further simplified as under.

$$\frac{\partial}{\partial x}\left(\frac{F_x}{\sqrt{F_x^2+F_y^2}}\right)+\frac{\partial}{\partial y}\left(\frac{F_y}{\sqrt{F_x^2+F_y^2}}\right)=0 \text{ in } \Omega \text{ for } t>0\ (x,y)\epsilon R^2, \quad (4)$$

which is non-linear and non-differentiable.

The time depended EL- PDE from equation (4) is given below.

$$\frac{\partial u}{\partial t}=\frac{\partial}{\partial x}\left(\frac{F_x}{\sqrt{F_x^2+E_y^2}}\right)+\frac{\partial}{\partial y}\left(\frac{F_y}{\sqrt{F_x^2+F_y^2}}\right). \quad (5)$$

For further details, see [25].

Radial Basis Function (RBF) Interpolation

Let us discuss the RBF approach [18]. RBF is a real valued function whose value depend only on the distance from the origin, so that $\psi(P)=\psi(\|P\|)$, or alternatively on the distance from some other point P^c, called center taken based through a stencil value n around a known center P^c , so that $\psi(P,P^c)=\psi(\|P-P^c\|)$. Any function ψ that satisfied the property $\psi(P)=\psi(\|P\|)$ is called RBF. The RBF method is used to interpolate smooth function, $f(P), P\in\Omega\subseteq R^n$, where Ω is the bounded domain for N evaluation data points $\{P_i,f_i\}_{i=1}^N\in R^n$. Let $\{P_j,F_j\}_{j=1}^M\in R^n$ be M center data points taking from evaluation N points, i.e. $M\leq N$. Now for $\{P_j^c,F_j\}_{j=1}^M\in R^n$ both center and evaluation points. The RBF approximation is defined as

$$\sum_{i=1}^M ß_J\psi(\|P_i^c-P_j^c\|)=F_j \quad ,for\ i,j=1,2,\dots M \quad (6)$$

The equation (6) leads to the following linear system.

$$\begin{bmatrix}\psi(\|P_1^c-P_1^c\|) & \psi(\|P_1^c-P_2{}^c\|) & \cdots & \psi(\|P_1^c-P_M^c\|)\\ \psi(\|P_2{}^c-P_1^c\|) & \psi(\|P_1^c-P_2^c\|) & \dots & \psi(\|P_2^c-P_M^c\|)\\ \vdots & \vdots & \vdots & \vdots\\ \psi(\|P_M^c-P_1^c\|) & \psi(\|P_M^c-P_2^c\|) & \dots & \psi(\|P_M^c-P_M^c\|)\end{bmatrix}\begin{bmatrix}L_1\\L_2\\\vdots\\L_M\end{bmatrix}=\begin{bmatrix}F(P_1)\\F(P_2)\\\vdots\\F(P_M)\end{bmatrix}. \quad (7)$$

In matrix notation, the above system (7) can be written as

$$AL=F \quad (8)$$

Where $L=(L_1,L_2,L_3\dots..L_M)^t$, $f=(F_1,F_2,F_3,\dots\dots.F_M)^t$ are M×1 matries and L is to be

Dialogue Social Science Review (DSSR)
www.thedssr.com

ISSN Online: 3007-3154
ISSN Print: 3007-3146

DIALOGUE SOCIAL SCIENCE REVIEW

Vol. 3 No. 2 (February) (2025)

determined in it and $A = [\psi_{ij}] = (A_{ij}) \epsilon R^{N\times N}$ is M×M matrix called interpolation or system matrix.

The above equation (8) can be further defined as under by similar way as done in [53].

$$L = A^{-1}F \tag{9}$$

Now N evaluation points $\{P_i, F_i\}_{i=1}^{N} \in R^n$ and M center points $\{P_j^c, F_j\}_{j=1}^{M} \in R^n$, again the RBF approximation will become,

$$\sum_{i=1}^{N} L_j \psi(\|P_i - P_j^c\|) \quad , for\ i = 1,2, \dots N, J = 1,2,3 \dots M, \tag{10}$$

The above equation leads to the following N× M matrix

$$\begin{bmatrix} \psi(\|P_1 - P_1^c\|) & \psi(\|P_1 - P_2^c\|) & \cdots & \psi(\|P_1 - P_M^c\|) \\ \psi(\|P_2 - P_1^c\|) & \psi(\|P_2 - P_2^c\|) & \dots & \psi(\|P_2 - P_M^c\|) \\ \vdots & \vdots & \vdots & \vdots \\ \psi(\|P_N - P_1^c\|) & \psi(\|P_N - P_2^c\|) & \dots & \psi(\|P_N - P_M^c\|) \end{bmatrix} \begin{bmatrix} L_1 \\ L_2 \\ \vdots \\ L_M \end{bmatrix} = \begin{bmatrix} F_0(k_1) \\ F_0(k_2) \\ \vdots \\ F_0(k_M) \end{bmatrix}. \tag{11}$$

The above matrix system (11) results in the following system of equations.

$$F_0 = CL, \tag{12}$$

where $C = [\psi_{ij}] = (C_{ij}) \epsilon R^n = \sum_{i=1}^{N} L_j \psi(\|P_i - P_j^c\|)$, is called evaluation matrix.

Put equation (9) in equation (12)

$$E_0 = CA^{-1}F \tag{13}$$

Let $A^{-1}F = D$ (14)

Then equation (14) become

$$F_0 = CD. \tag{15}$$

Where D is N × 1 matrix.

For more information, see [18]

Numerical Schemes For TV –Based Edge Detection Model

This section discusses numerical methods for solving the non-linear PDE (5) related to the minimization functional (2), which is used for edge detection.

Implicit Gradient Descent Method (M1)

EL-PDE from (5) in model [27] is given as under.

$$\frac{\partial F}{\partial t} = \left(\frac{F_{xx}}{\sqrt{F_x^2 + F_y^2}}\right) + \left(\frac{F_{yy}}{\sqrt{F_x^2 + F_y^2}}\right). \tag{16}$$

The implicit gradient descent method is applied on (16) and obtained the following

Dialogue Social Science Review (DSSR)
www.thedssr.com

ISSN Online: 3007-3154
ISSN Print: 3007-3146

DIALOGUE SOCIAL SCIENCE REVIEW

Vol. 3 No. 2 (February) (2025)

equations.

$$\frac{F^{(k+1)}-F^{(k)}}{dt} = \frac{F^{(k)}{}_{xx}}{\sqrt{(F_x^2)^k+(F_y^2)^k}} + \frac{F^{(k)}{}_{yy}}{\sqrt{(F_x^2)^k+(F_y^2)^k}}, \quad (17)$$

$$F^{(k+1)} = F^{(k)} + dt\left(\frac{F^{(k)}{}_{xx}+F^{(k)}{}_{yy}}{\sqrt{(F_x^2)^k+(F_y^2)^k}}\right), \quad (18)$$

$$F^{(k+1)} = \frac{E^{(k)}\left(\sqrt{(F_x^2)^k+(F_y^2)^k} + dt(F^{(k)}{}_{xx}+F^{(k)}{}_{yy})\right)}{\sqrt{(F_x^2)^k+(F_y^2)^k}}, \quad (19)$$

$$(F^{(k+1)})\sqrt{(F_x^2)^k + (F_y^2)^k} = F^{(k)}\left(\sqrt{(F_x^2)^k + (F_y^2)^k} + dt(F_{xx}^k + F_{yy}^k).\right. \quad (20)$$

$$\text{Let } L(F) = \sqrt{(F_x^2)^k + (F_y^2)^k} \quad (21)$$

put in equation (21) in equation (20), then

$$L(F^{(k)})(F^{(k+1)}) = F^{(k)}L(F) + dt\left(F_{xx}^{(k)} + F_{yy}^{(k)}\right) \quad (22)$$

For more information see [25]

Proposed Meshless Method (M2)

This subsection introduces the Local Meshless Method (LMM) for efficient numerical simulation of the EL-PDE described in equation (5) related to the model in equation (2). The proposed LMM not only reconstructs the images effectively but also preserves sharp edges due to its adaptive characteristics, computational efficiency, and its mesh-free implementation using Multiquadric Radial Basis Functions (MQ-RBF). As a result, the PSNR and EPI values will consistently improve when utilizing the proposed meshless method. Assume $\{P_i, F_i\}_{i=1}^{N}$ be N_c data centers in a closed domain $\Omega \subseteq R^2$ with RBF equation $\psi(r) = \|r\|_2$ in R^2, i.e., $r = (x, y)$. Thus, the polynomial term free RBF interpolation for the provided known $\{P_j^c, F_j\}_{j=1}^{N}$ data points is expressed as follows.

$$T(k) = \sum_{i=1}^{N_c} L_j \psi(\|P_i^c - P_j^c\|_2) \quad \text{for i, j=1.2.3..., } N_c. \quad (23)$$

The coefficient of L_J is found from equation (23) using the subsequent interpolation condition.

$$T(P_i) = Ⱨ_Ɔ, , \quad (24)$$

with a group of points which agree to centers points N_c. The RBF interpolation at N_c data centers is presented through the given over determined interpolation form:

$$AL = Ⱨ_Ɔ, \quad (25)$$

which give rise to $N_c \times N_c$ system of linear equations, which is responsible to evaluate co-efficient L, where $L = (L_1, L_2 \ldots L_{Nc})^t$ and $f = (Ⱨ_{Ɔ1}, Ⱨ_{Ɔ2} \ldots Ⱨ_{ƆNc})^t$ represent $N_c \times 1$ order matrices. In equation (25), matrix A is acknowledged as $N_c \times N_c$ square

Dialogue Social Science Review (DSSR)
www.thedssr.com

ISSN Online: 3007-3154
ISSN Print: 3007-3146

DIALOGUE SOCIAL SCIENCE REVIEW

Vol. 3 No. 2 (February) (2025)

interpolation matrix also called system matrix. Matrix A can be represented as follow.

$$A = [\psi_{ij}] = \left[\psi\left(\left\|P_i^c - P_j^c\right\|_2\right)\right]_{1\le i,j\le N_c}. \quad (26)$$

In equation. (25) matrix A is invertible [58] and positive definite which have critical aspect for unique solution of Equation. (25). Thus

$$L = A^{-1}Ң. \quad (27)$$

Furthermore, at $\{P_i\}_{i=1}^{N}$ N evaluation data points and $\{P_i\}_{i=1}^{N_c}$ N_c center points, the RBF interpolation by applying Equation (23) generates $N \times N_c$ matrix C which is written as follows.

$$C = [\psi_{ij}] = \left[\psi\left(\left\|P_i - P_j^c\right\|_2\right)\right] \quad for\ i = 1, 2, 3, \dots, N, and\ j = 1, 2, 3 \dots, N_c\ . \quad (28)$$

Additionally, using the matrix-vector product to obtain F, the interpolation over the selected condition is approximated for N data points and is explained as follows.

$$F = CL. \quad (29)$$

Combining equation (27) and (29) result in the given equation.

$$F = CA^{-1}Ң, \quad (30)$$

or

$$F = DҢ \quad where\ D = CA^{-1}. \quad (31)$$

This gives an estimate of the answer at any given location in Ω. Since the time marching restoration PDE [25] from equation (5) is mentioned by the following equation, where F is of N×1 order matrix.

$$\frac{du}{dt} = \frac{\partial}{\partial x}\left(\frac{F_x}{\sqrt{F_x^2+F_y^2}}\right) + \frac{\partial}{\partial y}\left(\frac{F_y}{\sqrt{F_x^2+F_y^2}}\right)\ in\ \Omega\ for\ t > 0\ (x,y)\epsilon R. \quad (32)$$

Using the specified F(x, y, 0) with boundary condition $\frac{\partial F}{\partial n}$=0 on $\partial\Omega$ .The following is an improved version of equation (32).

$$\frac{dF}{dt} = \frac{(F_{xx}+F_{yy})(F_x^2+F_y^2)-(2F_xF_yF_{xy}+F_x^2F_{xx}+F_y^2F_{yy})}{(F_x^2+F_y^2)^{\frac{3}{2}}}\ . \quad (33)$$

The restoration equation (33) and the value from (31) are combined to create a nonlinear restoration system of equations that can be solved using the Implicit Gradient Descent iterative approach.

$$\frac{F^{(n+1)}-F}{dt} = \frac{(F^{(n)}{}_{xx}+F^{(n)}{}_{yy})((F_x^2)^{(n)}+(F_y^2)^{(n)})-(2F_x{}^{(n)}F_y{}^{(n)}(F_x{}^{(n)}F_y+F_xF_y{}^{(n)})+F^2{}_xF^{(n)}{}_{xx}+F^2{}_yF^{(n)}{}_{yy})}{((F_x^2)^n+(F_y^2)^n)^{\frac{3}{2}}}. \quad (34)$$

Equation (34) can further be simplified as under.

$$M\left(F^{(k)}\right)F^{(k+1)} = M\left(F^{(k)}\right)F^{(k)} + dt[(F^{(k)}{}_{xx} + F_{yy}{}^{(k)})((F^2{}_x)^{(k)} + (F^2{}_y)^{(k)}-) - (2F^{(k)}{}_x\,F^{(k)}{}_y(\,F^{(k)}{}_xF_y + F_x\,F^{(k)}{}_y) + (F^2{}_x)^{(k)}\,F_{xx}{}^{(k)} + (F^2{}_y)^k\,F^{(k)}{}_{yy})], \quad (35)$$

where,

$$M(F) = \left(F^2{}_x + F^2{}_y\right)^{\frac{3}{2}},\ F_x = D_XҢ,\ F_y = D_yҢ,\ F_{xx} = D_{xx}Ң,\ and\ F_{yy} = F_{yy}Ң.$$

The LMM has greater flexibility in choosing a Radial Basis Function (RBF), allowing it

Dialogue Social Science Review (DSSR)
www.thedssr.com

ISSN Online: 3007-3154
ISSN Print: 3007-3146

DIALOGUE SOCIAL SCIENCE REVIEW

Vol. 3 No. 2 (February) (2025)

to effectively fulfill the resulting EL-PDE (35). The most commonly used RBF in LMM is the Multiquadric Radial Basis Function (MQ-RBF), which generally achieves spectral accuracy when the shape parameter c is appropriately selected. This selection is entirely dependent on the image size and noise level.

Algorithm for LMCT (M2)
RBF interpolation;

1. Select $N = N_c$, n number of data pixel points.
2. Determine L according to the equation (27) by MQ-RBF.
3. Calculate F by using equation (31) by applying MQ-RBF.

TV regularization;

4. Select the values for c, dt and Ⱨ, ϵ.
5. Pick n N_c quantity of data pixel centers i.e. $P_{c1} \leq P_{c2} \leq \cdots P_{cn}$ from N data points next choose n=0.
6. Replace E as Local RBF utilizing equation (31) in equation (35).
7. Select $n = n + 1$ for each data center point k_{ci}, for $1 \leq i \leq N$, then compute $E^{(n+1)}$ according the equation (35) by LMM, where $Ⱨ^{(0)} = Ⱨ$.
8. $\frac{\|F^{(n+1)} - F^{(n)}\|}{\|F^{(n)}\|} \leq \boldsymbol{\varepsilon = 10\text{^} - 5}$, criteria is utilized to break the iterative process. If no, move gain to step 7.
9. End.
10. Output result $F = F^{(n+1)}$

Experimental Analysis

This section presents experimental findings and analyses conducted on various images, specifically Fingerprint, Rice, and Lena, to evaluate the performance of the proposed meshless algorithm, M2. Grayscale images are used to assess the effectiveness of both M1 and M2. The test images are displayed in Figure 1. Salt and pepper noise significantly degrades image details, leading to challenges in performing image processing tasks such as edge detection, image segmentation, and face recognition. In this study, we compare edge detection in test images containing Salt and Paper noise with mean $\mu = 0$, $variance\ p$. In order to verify the picture restoration outcomes of proposed LMM M2 and compare its results with traditional mesh-based method M1. We select the image size with $N = N_c =$ size of the image and use the suggested LMM M2. Peak-to-noise ratio (PSNR) is taken into consideration to quantify the denoised image. This measure is widely used to evaluate the quality of the restored image. PSNR is calculated as

$$\text{PSNR}=10 \times log_{10}\left(\frac{p \times qmax\{E_0\}^2}{\|E_0 - E\|^2}\right), \quad (36)$$

Where F_0 is the final denoised image, $p \times q$ denotes the image data size, and F is the original images that were provided. Greater the PSNR value better will be the restoration performance.

By choosing the best Regions of Interest, the Edge Preserving Index (EPI) is utilized to determine the edge's quality. The EPI range typically lies between 0 and 1, where a

Dialogue Social Science Review (DSSR)
www.thedssr.com

ISSN Online: 3007-3154
ISSN Print: 3007-3146

DIALOGUE SOCIAL SCIENCE REVIEW

Vol. 3 No. 2 (February) (2025)

blurry edge inside the Region of Interest (ROI) corresponds to a lower EPI value and vice versa. Therefore, the following equation is used to estimate the EPI value for the mth ROI.

$$EPI = \frac{1}{M}\sum_{m=1}^{M} \frac{\Gamma(Ⱨ_m - \overline{Ⱨ_m}, F_m - F_{0_m})}{\sqrt{\Gamma(Ⱨ_m - \overline{Ⱨ_m}, F_{0_m} - F_{0_m})}}, \quad (37)$$

where, M is considered the total number of regions, $Ⱨ_m$ the noisy ROI region, and E_{0_m} is the denoised ROI region. We refer to $\overline{Ⱨ_m}$ as the empirical mean $Ⱨ_m$. Within the ROI's defined range, Γ is considered the correlation and is expressed as follows:

$$\Gamma(Ⱨ_1, F_{0_m}) = \sum_{i,j \epsilon ROI} Ⱨ_1(i,j).F_{0_m}(i,j). \quad (38)$$

The EPI value near to 1 leads to the good edge preservation property. The suggested scheme M2's faster convergence achievement and the stoppage of the iterative procedure are represented by the following formula.

$$\frac{\|F^{k+1} - F^k\|}{\|F^k\|} \leq \varepsilon \ , \quad (39)$$

where $\varepsilon = 10^{-5}$ gives the maximum amount of error allowed. (MQ-RBF) is chosen in the suggested algorithm M2 as a basis function. Every selected point (x_j, y_j) has the following MQ-RBF expression:

$$\psi_j(x,y) = \sqrt{c^2 + ((x - x_j)^2 + (y - y_j)^2)} \ , \quad (40)$$

where

$$r^2{}_j = (x - x_j)^2 + (y - y_j)^2$$

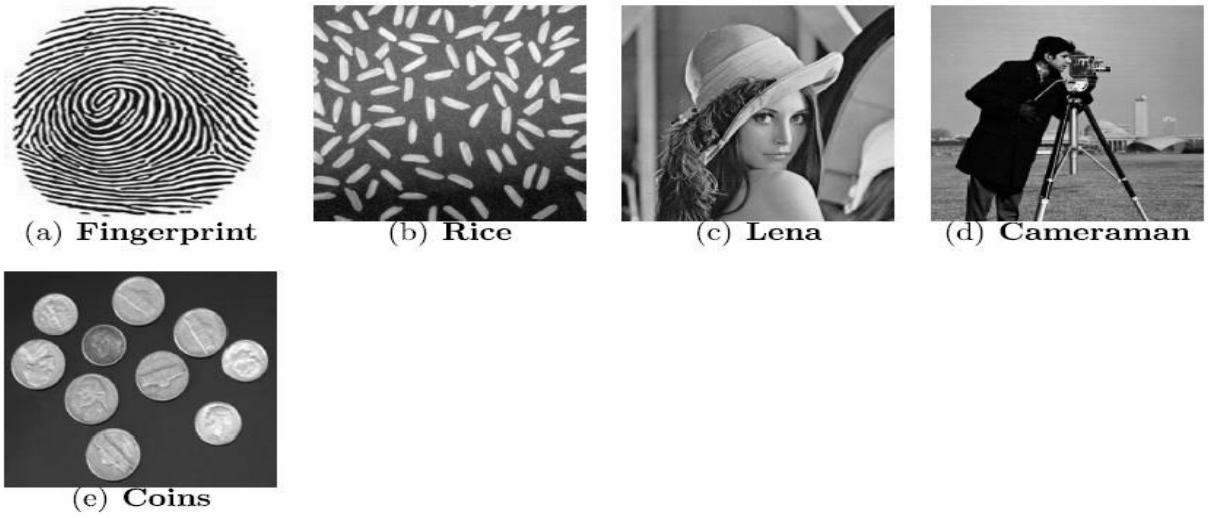

(a) Fingerprint (b) Rice (c) Lena (d) Cameraman (e) Coins

Figure 1: Test images for edge detection

Dialogue Social Science Review (DSSR)
www.thedssr.com

ISSN Online: 3007-3154
ISSN Print: 3007-3146

DIALOGUE SOCIAL SCIENCE REVIEW

Vol. 3 No. 2 (February) (2025)

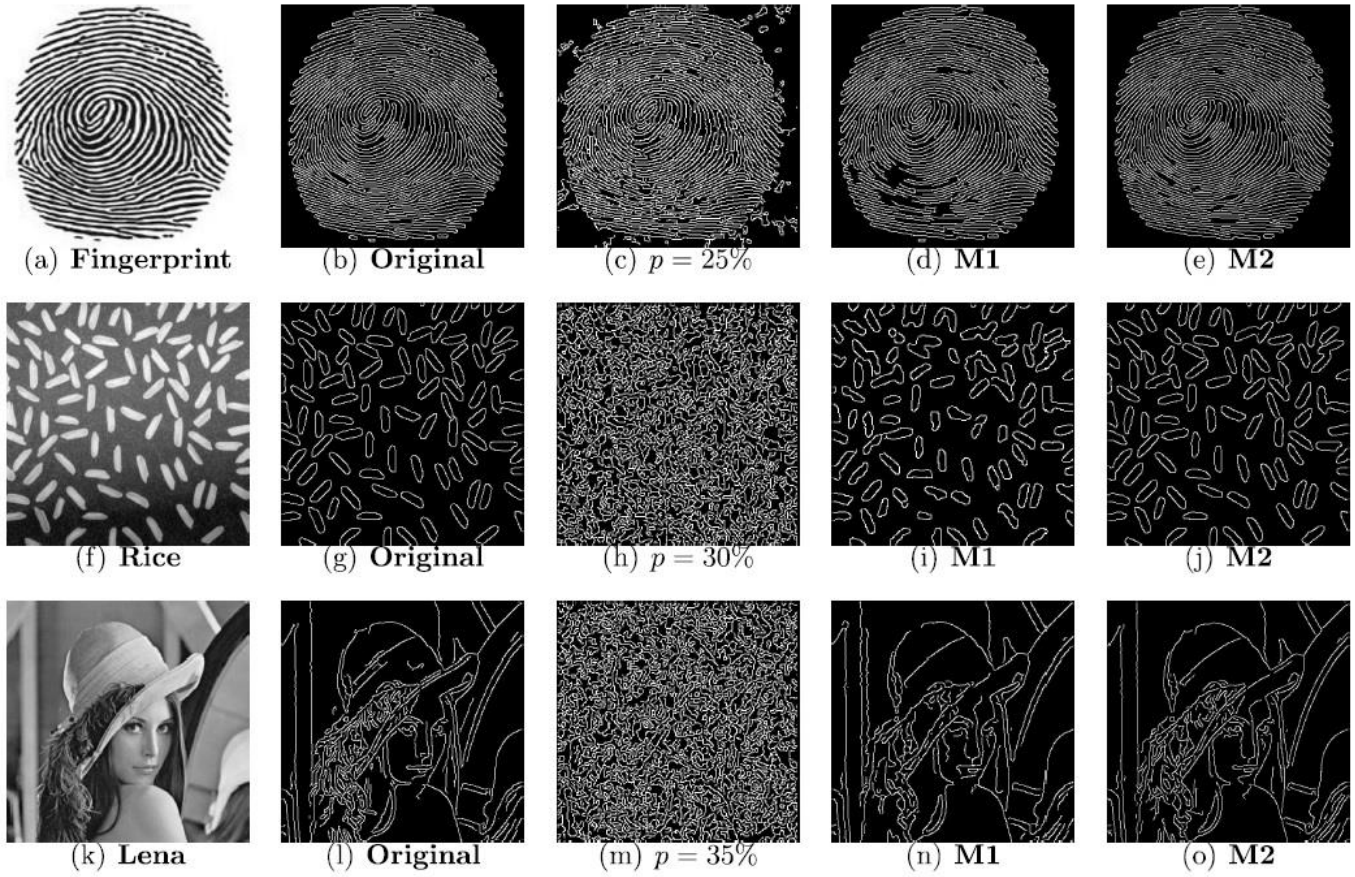

Fig: 2 Comparison of edge detection and image restoration performance of Fingerprint, Rice, and Lena images; (a) Given test image Fingerprint; (b) Edge based test image; (c) Edge based based noisy image containing salt and paper noise p=25%; (d) Restored by M1 method; (e) Restored by Proposed M2 method with c=1.09. (f) Test image Rice; (g) Edge based test image; (h) noisy edge-based image having salt and paper noise p=30%; (i) Obtained image using M1 method; (j) Obtained image using M2 proposed method with c=1.15. (k) Test image Lena; (l) Edge based test image; (m) Edge based noise image with salt and paper noise p=35%; (n) Resultant image by M1; (o) Resultant image by M2 with c=1.18.

Table1: Analysis of the PSNR and EPI values for techniques M1 and M2.

Image	Size	Technique M1		Technique M2	
		EPI	PSNR	EPI	PSNR
Fingerprint	256^2	0.649	23.21	0.701	23.73
Rice	256^2	0.695	24.27	0.749	24.89
Lena	256^2	0.71	25.36	0.763	25.87

Dialogue Social Science Review (DSSR)
www.thedssr.com

ISSN Online: 3007-3154
ISSN Print: 3007-3146

DIALOGUE SOCIAL SCIENCE REVIEW

Vol. 3 No. 2 (February) (2025)

Table 2: Analysis of two schemes M1 and M2 in terms of CUP time in seconds and number of iterations.

Image	Scheme M1		Scheme M2	
	Iteration	Time(s)	Iteration	Time(s)
Fingerprint	28	11.02	13	8.19
Rice	18	9.21	10	6.83
Lena	14	8.39	8	5.44

Experiment

In this first comparison, we compare the two mesh-based method M1 and mesh-based method M2 for edge detection on three images i.e., Fingerprint, Rice, and Lena having salat and paper noise with noise variances p=25%, 30%, and 35%, respectively which are shown in Figure 2. In Figure. 2, (a)-(b), (f)-(g), and (k)-(i) represent the original and its respective edge-based images, receptively. Figure reviled that the image edge detection obtained by the suggested meshless approach M2 is for better than M1. M1 also results in good edge detection outcome because of the TV regularization used in it which is the inherent application of TV regularization. But due to the associated second order Euler Lagrange PDE, it becomes anisotropic regularization-based filter which gives best edge detection results compared to the traditional filters [27]. But due to the nonlinearity and differentiability of associated PDE, sometimes the traditional mesh-based method M1 is struggling with smooth solution regarding edge detection i.e., weak and discontinuous edge detection results and hence also produced poor restoration results. These results are listed in Figure. 2 as (d), (i), and (n), respectively for the three test images Fingerprint, Rice, and Lena. However, the meshless algorithm M3 produces more effective image restoration (edge detection and denoising) results compared to the traditional method M1 due to a mesh-free feature, adaptive nature, MQ-RBF approximation, and the smooths the solution of the PDE associated with the TV regularization-based model by meshless method M2. These reconstructed results are displayed in Figure. 2 as (e), (j), and (o), respectively of the three test images. Furthermore, Table. 1 presents that EPI and PSNR values of M2 are greater than M1 which demonstrate the best restoration performance of algorithm M2 over algorithm M1 regarding the edge detection and denoising for all the three test images Fingerprint, Rice, and Lena. It can also be seen from Table. 2 that the computation time (CPU) and number of iterations needed for convergence approach M2 are lower than in approach M1 due to the computational efficiency nature of the meshless method M2. Hence the proposed meshless method M2 produces quick restoration performance than traditional mesh-based method M1.

Conclusion

This article introduces the Local Meshless Method (LMM) for the numerical solution

ISSN Online: 3007-3154
ISSN Print: 3007-3146

Vol. 3 No. 2 (February) (2025)

of edge detection in a Total Variation (TV) model connected to the enhancement of images through smoothing and salt-and-pepper denoising. The LMM offers several advantages, including quick, high-quality restoration performance in both edge detection and denoising. Its benefits arise from its meshless and adaptive nature, the use of Multiquadric Radial Basis Functions (MQ-RBF) as the basis function, and its computational efficiency The associated meshless scheme was tested on various images and its results were compared with those obtained from traditional methods and filters. The experimental results revealed that the proposed meshless method (LMM) significantly outperforms many traditional methods in image restoration, specifically in edge detection and denoising, as indicated by improved EPI and PSNR values, as well as reduced CPU time.

References

1. Olson, C.F., Hutten ocher, D.P., 1997. Automatic target recognition by matching oriented edge pixels. IEEE Transactions on Image Processing 6, 103–113.
2. Du, J.X., Huang, D.S., Wang, X.F., Gu, X., 2007. Shape recognition based on neural networks trained by differential evolution algorithm. Neuro computing 70, 896–903.
3. Vu, N.S., Caplier, A., 2011. Enhanced patterns of oriented edge magnitudes for face recognition and image matching. IEEE Transactions on Image Processing 21, 1352–1365.
4. Drolia, U., Guo, K., Tan, J., Gandhi, R., Narasimhan, P., 2017. Cachier: Edge-caching for recognition applications, in: 2017 IEEE 37th international conference on distributed computing systems (ICDCS), pp. 276–286.
5. Ramadevi, Y., Sridevi, T., Poornima, B., Kalyani, B., 2010. Segmentation and object recognition using edge detection techniques. AIRCC's International Journal of Computer Science and Information Technology 2, 153–161.
6. Wei, Y., Liang, X., Chen, Y., Shen, X., Cheng, M.M., Feng, J., Zhao, Y., Yan, S., 2016. STC: A simple to complex framework for weakly supervised semantic segmentation. IEEE Transactions on Pattern Analysis and Machine Intelligence 39, 2314–2320.
7. Wang,X.F.,Huang,D.S., Xu,H.,2010. Anefficient local chan–vese model for image segmentation. Pattern Recognition 43, 603–618.
8. Jing, J., Liu, S., Wang, G., Zhang, W. and Sun, C., 2022. Recent advances on image edge detection: A comprehensive review. *Neurocomputing*, *503*, pp.259-271.
9. Pavithra, L., Sharmila, T.S., 2018. An efficient framework for image retrieval using color, texture and edge features. Computers & Electrical Engineering 70, 580–593.
10. Li, B., Huang, D.S., Wang, C., Liu, K.H., 2008a. Feature extraction using constrained maximum variance mapping. Pattern Recognition 41, 3287–3294.
11. Zhao, Z.Q., Huang, D.S., Sun, B.Y., 2004. Human face recognition based on multi-features using neural networks committee. Pattern recognition letters 25, 1351–1358.
12. Chen, W.S., Yuen, P.C., Huang, J.,Dai,D.Q.,2005. Kernelmachine based one-parameter regularized Fisher discriminant method for face recognition. IEEE Transactions on Systems, Man, and Cybernetics, Part B (Cybernetics) 35, 659–669.

ISSN Online: 3007-3154
ISSN Print: 3007-3146

Vol. 3 No. 2 (February) (2025)

13. Li, B., Zheng, C.H.,Huang,D.S.,2008b. Locally linear discriminant embedding: An efficient method for face recognition. Pattern Recognition 41, 3813–3821.
14. Zhang, W.C., Wang, F.P., Zhu, L., Zhou, Z.F., 2014. Corner detection using Gabor filters. IET Image Processing 8, 639–646.
15. Zhang, W., Shui, P., 2015. Contour-based corner detection via angle difference of principal directions of anisotropic Gaussian directional derivatives. Pattern Recognition 48, 2785–2797.
16. Dollar, P., Tu, Z., Belongie, S., 2006. Supervised learning of edges and object boundaries, in: Proceeding of the IEEE Conference on Computer Vision and Pattern Recognition, pp. 1964–1971.
17. Leal-Taixé, L., Canton-Ferrer, C., Schindler, K., 2016. Learning by tracking: Siamese CNN for robust target association, in: Proceedings of the IEEE Conference on Computer Vision and Pattern Recognition, pp. 33–40.
18. Baştan, M., Bukhari, S.S., Breuel, T., 2017. Active Canny: edge detection and recovery with open active contour models. IET Image Processing 11, 1325–1332.
19. Haddad, A. and Meyer, Y., 2007. An improvement of Rudin–Osher–Fatemi model. Applied and Computational Harmonic Analysis, 22(3), pp.319-334.
20. M.A Khan., Chen, W., Ullah, A. and Fu, Z., 2017. A mesh-free algorithm for ROF model. EURASIP Journal on Advances in Signal Processing, 2017, pp.1-16.
21. Wu, X., Zheng, J., Cai, Y. and Fu, C.W., 2015, October. Mesh denoising using extended ROF model with L1 fidelity. In Computer Graphics Forum (Vol. 34, No. 7, pp. 35-45).
22. Rudin, L., Osher, S., Fatemi, E.: 'Nonlinear total variation based noise removal algorithms', Physica D, 1992, 60, pp. 259–268
23. D Krishnan, P Lin, XC Tia, An efficient operator-splitting method for noise removal in images. Commun. Comput. Phys. 1(5), 847–858 (2009)
24. L Rudin, S Osher, Total variation based image restoration with free local constraints. IEEE Trans. Image Process. 1, 31–35 (1994). doi:10.1109/ICIP.1994.413269.
25. Ndajah, P. and Kikuchi, H., 2011, February. Total variation image edge detection. In Proceedings of the 10th WSEAS International Conference on Electronics, Hardware, Wireless and Optical Communications (pp. 246-251).
26. T Goldstein, S Osher, The split bregman method for L1-regularized problems. SIAM J. Imaging Sci. 2(2), 323–343 (2009). doi:10.1137/080725891.
27. DH Jiang, X Tan, YQ Liang, S Fang, A new nonlocal variational bi regularized image restoration model via split bregman method. EURASIP. J Image. Vide. Process. 15(1) (2015). doi:10.1186/s13640-015-0072-7.
28. X Liu, L Huang, A new nonlocal total variation regularization algorithm for image denoising. Math. Comput. Simulat. 97(1), 224–233 (2014). doi:10.1016/j.matcom.2013.10.001
29. XLiu, L Huang, An efficient algorithm for adaptive total variation based image decomposition and restoration. Int. J Appl. Comput. Sci. 24(2), 405–415 (2014). doi:10.2478/amcs-2014-0031.

Dialogue Social Science Review (DSSR)
www.thedssr.com

ISSN Online: 3007-3154
ISSN Print: 3007-3146

DIALOGUE SOCIAL SCIENCE REVIEW

Vol. 3 No. 2 (February) (2025)

30. XLiu, L Huang, Total bounded variation-based Poissonian images recovery by split bregman iteration. Math. Method. Appl. Sci. 35(5), 520–529 (2012). doi:10.1002/mma.1588.
31. XCTai, C Wu, Augmented lagrangian method, dual methods, and split bregman iteration for ROF model. SSVM Springer. 5567, 502–513 (2009). doi:10.1007/978-3-642-02256-2-42.
32. HXu, QSun, NLuo, GCao, DXia, Iterative nonlocal total variation regularization method for image restoration. PLOS ONE. 8(6), e65865 (2013). doi:10.1371/journal.pone.0065865.
33. EJ Kansa, Multiquadrics-a scattered data approximation scheme with applications to computational fluid dynamics I: solutions to parabolic, hyperbolic, and elliptic partial differential equations. Comput. Math. App. 19, 147–161 (1990). doi:10.1016/0898-1221(90)90270-T
34. EJ Kansa, Multiquadrics-a scattered data approximation scheme with applications to computational fluid dynamics II: surface approximations and partial derivative estimates. Comput. Math. App. 19, 127–145 (1990). doi:10.1016/0898-1221(90)90271-K.
35. Khan, M.A., Altamimi, A.B., Khan, Z.H., Khattak, K.S., Ali, M., Ullah, A., Khan, S., Khan, M.S. and Abrar, M.F., 2020. Total Variation Filter via Multiquadric Radial Basis Function Approximation Scheme for Additive Noise Removal. *IEEE Access*, *8*, pp.88241-88258.
36. Nair, M.S. and Raju, G., 2011. Additive noise removal using a novel fuzzy-based filter. *Computers & Electrical Engineering*, *37*(5), pp.644-655.
37. Khan, M.A., Chen, W., Ullah, A. and Fu, Z., 2017. A mesh-free algorithm for ROF model. *EURASIP Journal on Advances in Signal Processing*, *2017*, pp.1-16.
38. M. D. Buhmann, *Radial Basis Functions: Theory and Implementations*, vol. 2. Cambridge, U.K.: Cambridge Univ. Press, 2003.
39. W. Z. J. Chen Fu and C. S. Chen, *Recent Advances in Radial Basis Function Collocation*. Berlin, Germany: Springer-Verlag, 2013, doi: 10.1007/978-3- 642-39572-7.
40. Tominec, I. and Breznik, E., 2021. An unfitted RBF-FD method in a least-squares setting for elliptic PDEs on complex geometries. *Journal of Computational Physics*, *436*, p.110283.
41. TA Driscoll, B Fornberg, Interpolation in the limit of increasingly flat radial basis functions. Comput. Math. App. 3-5(43), 413–422 (2002). doi:10.1016/j.jcp.2015.12.01.
42. M Zerroukat, H Power, CS Chen, A numerical method for heat transfer problem s(1998). doi:10.1002/(SICI)1097-0207
43. (EJ Kansa, ed.), Motivation for using radial basis functions to solve PDEs. (LLNL, USA, 1999). doi:10.1007/s11075-012-9675-6
44. JLi, YC Hon, Domain decomposition for radial basis meshless methods. IEEE Trans. Commun. 31, 388–397 (1983). doi:1002/num.10096
45. E Larsson, B Fornberg, A numerical study of some radial basis function based solution methods for elliptic PDEs. Comp. Math. Appl. 46, 891–902 (2003). doi:10.1016/S0898-1221(03)90151-9

ISSN Online: 3007-3154
ISSN Print: 3007-3146

Vol. 3 No. 2 (February) (2025)

46. F Bernal, G Gutiérrez, Solving delay differential equations through RBF collocation.AAMM.1(2),257–272(2009).doi:arXiv:1701.00244
47. Buhmann, M., Dyn, N. (1993). Spectral convergence of multiquadric interpolation. *Proceedings of the EdinburghMathematical Society, 36(2),* 319–333. DOI 10.1017/S0013091500018411.
48. Sarra, S. A. (2009). Multiquadric radial basis function approximation methods for the numerical solution of partial differential equations. Artical, Marshall University and Edward J. Kansa University of California, USA.
49. Y Chen, S Gottlieb, A Heryudono, A Narayan, A reduced radial basis function method for partial differential equations on irregular domains. J. Sci.Comp.Arc.66(1),67–90(2016).doi:10.1007/s10915-015-0013-8
50. M Dehghan, M Abbaszadeh, A Mohebbi, A meshless technique based on local radial basis functions collocation method for solving parabolic-parabolic-patlak-keller-**segal-chemotaxis model.Eng.Anal.Bound.156,129-144 (2015). doi:10.1016/j.enganabound.2015.02.005**
51. SU Islam, V Singh, S Rajput, Estimation of dispersion in an open channel from an elevated source using an upwind local meshless method. Inter. J. Comp. Meth (2016). In Press, doi:10.1142/S0219876217500098
52. SU Islam, B Sarler, R Vertnik, Local radial basis function collocation method along with explicit time stepping for hyperbolic partial differential equations. Appl. Num. Math. 67, 136–151 (2013). doi:10.1016/j.apnum.2011.08.009
53. (K Liu, ed.), Radial basis functions: Biomedical applications and parallelization. Theses and Dissertations. (Ke Liu University of Wisconsin-Milwaukee, 2016)
54. S Sajavicius, Optimization, conditioning and accuracy of radial basis function method for partial differential equations with nonlocal boundary conditions. Eng. Anal. Bound. Elem. 37(4), 788–804 (2013). doi:10.1016/j.enganabound.2013.01.009.
55. M. D. Buhmann, *Radial Basis Functions: Theory and Implementations*, vol. 2. Cambridge, U.K.: Cambridge Univ. Press, 2003.
56. Hardy, R.L., 1971. Multiquadric equations of topography and other irregular surfaces. Journal of geophysical research, 76(8), pp.1905-1915.
57. A. Ali, S. U. Islam, S. Haq, Computational meshfree technique for the numerical solution of the two-dimensional coupled burgers equation Int J Compute methods ENG Sci Mesh. 10 406-412 (2009)
58. C. A Micchelli, Interpolation of scattered data: distance matrices and conditionally positive definite functions. Constr. Approx. 2, 11–12 (1986). doi:10.1007/BE01893414.